Novel target design for a laser-driven aneutronic fusion reactor

J. Gruenwald[a,*], C. Teodorescu[b]

[a] *Gruenwald Laboratories, Taxberg 50, 5660 Taxenbach, Austria*
[b] *American Institutes for Research, 1000 Thomas Jefferson St. NW, Washington, DC 20007, USA*

ABSTRACT

This paper discusses the suitability of proton sources and the appropriate targets for lithium-proton and boron-proton fusion reactions. Protons are emitted by a hydrogen-based source that is exposed to an intense laser beam. The protons are sent onto lithium or boron targets where fusion reactions are triggered. A comparison is made between solid, liquid and gaseous proton sources and the required laser intensity. Furthermore, the main characteristics of the lithium and boron targets are assessed. It is shown that a hybrid target made of lithium and boron offers opportunities to considerably enhance the fusion yield.

1. Introduction

This paper is a continuation of a previous work [1] that presented a small-scale fusion reactor in which aneutronic fusion reactions could be efficiently triggered in the gas phase. The device consists of a hybrid between a laser driven and an inertial electrostatic confinement (IEC) fusion reactor. IEC uses concentric, usually spherical electrodes to create conditions conducive of fusion reactions via strong electric fields [2,3]. Furthermore, it was argued that a hybrid reactor can overcome some of the challenges related to other fusion schemes, such as magnetic confinement or IEC, because it can be built much smaller than a tokamak or a stellarator. Also, the classical limit of confinement time in magnetic confinement fusion machines can be overcome by the application of brief laser pulses [1]. Since this hybrid reactor was proposed in 2017, it has been shown [4] that the number of fusion reactions on the cathode surface of an IEC device can exceed the number of fusion reactions in the gas phase by a factor of up to four, due to the high density of the embedded and absorbed hydrogen isotopes on the surface of the cathode. From this discovery, a further improvement of lithium-proton or boron-proton fusion reactors is presented in this work. The principal idea is that protons are accelerated by a high-intensity laser beam onto a lithium or a boron target where fusion reactions then occur. The lithium target will be liquid due to heating through the fusion reactions. The boron target, on the other hand, will stay solid because of its high melting temperature. The fusion-generated energy is transferred out of the reactor via water cooling, which keeps the target temperature constant. The steam created in the cooling process will then drive a steam turbine.

2. Fusion yield in lithium and boron

The two isotopes of lithium, ^{6}Li and ^{7}Li have a natural abundance of 7.4% and 92.6%, respectively. Both lithium isotopes can undergo fusion reactions with protons (p^+) according to the following reaction paths:

$$p^+ + {}^6\text{Li} \rightarrow {}^4\text{He} + {}^3\text{He} + 4.0\text{MeV} \tag{1}$$

$$p^+ + {}^7\text{Li} \rightarrow 2\,{}^4\text{He} + 17.2\text{MeV} \tag{2}$$

Since ^{7}Li is far more abundant and the energy yield per fusion reaction is much larger than for ^{6}Li all calculations in this paper will focus on reaction (2). The laser-accelerated protons are assumed to be monoenergetic and will move through vacuum until they hit the target. However, it will be demonstrated that even in the case of considerable energy spread the fusion yield can be conveniently maximised. In such a system the motion of the charged particles is not disturbed by any collisions and is only determined by the electric field generated by the laser beam. Thus, the fusion rate F is given by:

$$F \approx n_1 n_2 < \sigma v > . \tag{3}$$

Here n_1 and n_2 denote the densities of the particles involved, while $<\sigma v>$ is the reactivity. Note that in the case of monoenergetic proton beams there is no averaging needed for the calculation of the cross section σ and, subsequently, the reactivity. The density of the laser-accelerated protons will be discussed separately in the following section as the interplay between laser and proton source is more complicated. However, the density in the Li target can be obtained via the density of lithium, which is rather constant for solid Li but a function of the temperature for liquid Li, given by [5]:

$$\rho(T) = 562 - 0.1 \cdot T \tag{4}$$

* Corresponding author.
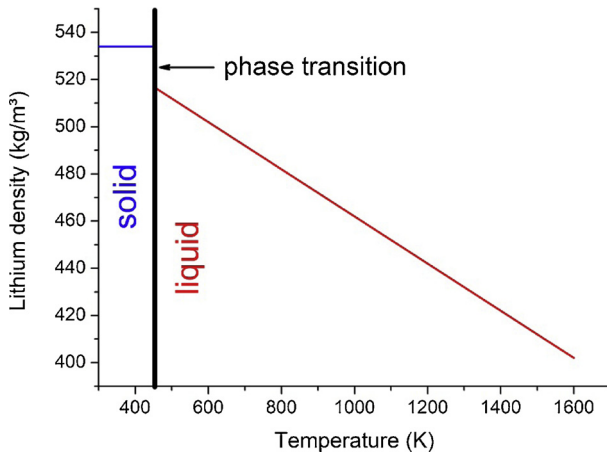*E-mail address:* jgruenwald@gmx.at (J. Gruenwald).

Fig. 1. Density of solid and liquid lithium.

where the temperature T has to be taken in K to obtain the density in kg/m^3. While solid Li has a density of about 534 kg/m^3, the temperature dependent density of liquid Li is shown in Fig. 1 in the range between the melting point of 453.7 K and the boiling point of 1603 K. As soon as the initially solid Li target is molten, we assume a steady state temperature of 1000 K, which corresponds to a density of 462 kg/m^3. This temperature is stabilised by active cooling. Subsequently, the particle density n_1 can be calculated with the mass of the Li atom (1.15×10^{-26} kg). $n_1 = 4.6 \times 10^{28}$ per m^3.

The cross section and reactivity for lithium-proton fusion reactions is depicted as a function of the incoming proton energy in Fig. 2. The maximum cross section is reached at a proton energy of 3 MeV, which corresponds to a cross section of $\sigma \approx 0.125$ barns. It has to be emphasised at this point that there is another local maximum in the cross section at around 6 MeV. However, at this value the cross section is smaller and the acceleration of protons with a laser requires over proportionally more laser power for 6 MeV than for 3 MeV.

Proton-boron fusion reactions, on the other hand, occur according to the following reaction path:

$$p^+ + {}^{11}B \rightarrow 3\,{}^4He + 8.7MeV \tag{5}$$

Since boron has a melting point of about 2350 K, a constant solid stat mass density of 2340 kg/m^3 is taken for the subsequent calculations [8]. The following Fig. 3 shows the cross section and reactivity for boron-proton fusion reactions:
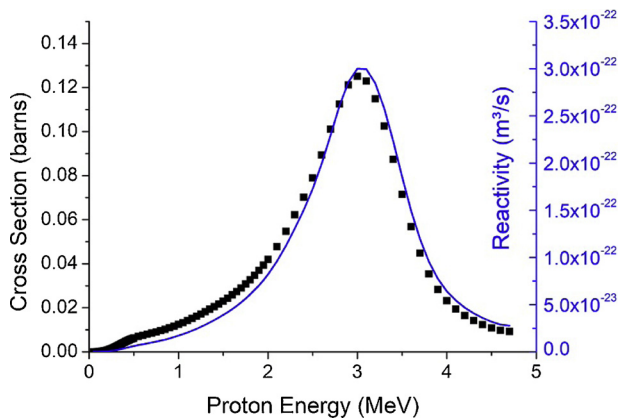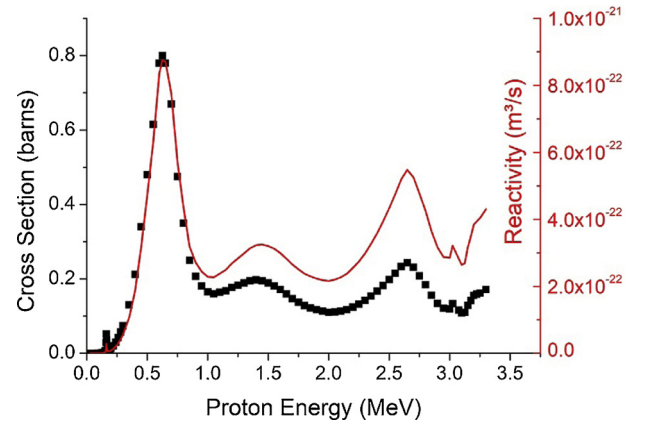

Fig. 3. Fusion cross section and reactivity for boron-proton fusion as a function of the proton energy. Data taken from the EXFOR database in the version of 17th December 2018 [6] and Ref. [7,9].

Table 1
Comparison of the properties of different hydrogen phases and their corresponding laser intensities.

Intensity (W/cm^2)	Phase	Proton energy (MeV)	Number of protons	Reference
10^{16}	Gaseous	1.1	$5 \cdot 10^9$	Palmer [10]
$10^{18} - 10^{21}$	Gaseous	0.6	10^6	Sharma [11]
10^{20}	Gaseous	0.7–1.5	$1.2 \cdot 10^{10}$	Helle [12]
$5 \cdot 10^{18}$	Liquid	2	10^8	Morrison [13]
$3 - 5 \cdot 10^{19}$	Liquid	1.1	$2 \cdot 10^{10}$	Gauthier [14]
$3 \cdot 10^{18}$	Solid	1.5	10^9	Maksimchuk [15]
$10^{17} - 10^{18}$	Solid	4	$10^{10} - 10^{11}$	Khaghani [16]
$3 \cdot 10^{16}$	Solid	0.3	10^{15}	Margarone [17]

3. Comparison of hydrogen-based proton sources

In the following Table 1 some values for the laser intensity, maximum proton energy and number of accelerated protons are compared from recent literature sources for different types of hydrogen phases: gaseous, liquid, solid.

Since it is not necessary to have protons with the highest kinetic energy but rather the largest amount of accelerated protons with energies that correspond to the maximum fusion cross section the following Fig. 4 shows the product of proton energy, number of
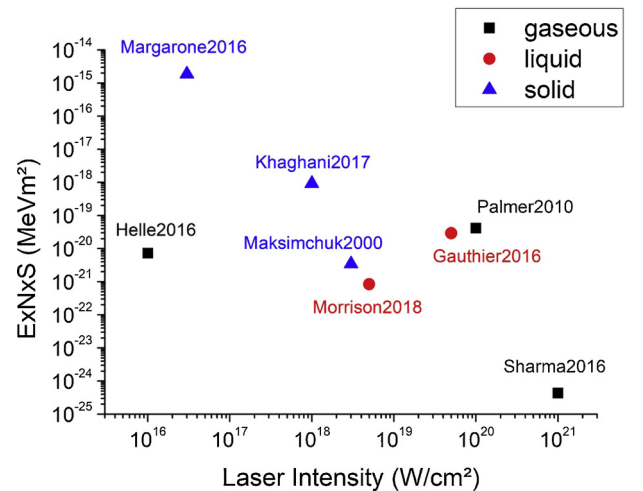

Fig. 2. Cross section and reactivity for the fusion reaction between protons and ^{7}Li atoms as a function of the proton energy. Data taken from the EXFOR database in the version of 17th December 2018 [6] and Ref. [7].

Fig. 4. Products of proton energy, proton number and fusion cross section at each of those energies for the data listed in Table 1. The different symbols and colors indicate the phase of the proton source.

accelerated protons and fusion cross section as a function of the laser intensity.

It is evident that the solid hydrogen phase used by Margarone et al. [17] provides the maximum value of about 3×10^{-15} MeV m^2 for a relatively small laser intensity of 3×10^{16} W/cm^2. The authors in this reference used the 600 Joule Prague Asterix Laser System (PALS) with sub nanosecond pulses. The laser beam was focused onto a spot with 80 μm diameter onto a 62 μm thick cryogenic hydrogen ribbon. It was found that after the impact of the laser pulse a plasma of around 200 μm length was formed on the rear side of the proton source. These data allow to estimate the proton density and, hence, the potential fusion rate for this type of reactor. The volume of the accelerated proton cloud is assumed to be a cylinder of 80 μm diameter and 200 μm length. This corresponds to a volume of about 10^{-12} m^3. Ref. [17] reports essentially the creation of slow protons with 0.4 MeV and fast protons with 1 MeV at the same time. Both of these species have sufficient energy to undergo fusion reactions in the solid lithium target but have different cross sections. The proton numbers for the fast and slow protons are 6.5×10^{14} and 5×10^{14}, respectively. The corresponding densities are, thus, around 6.5×10^{26} m^{-3} and 5×10^{26} m^{-3}, respectively.

Since the Li target can be made large enough so that beam spreading is not an issue and thick enough so that nearly all incoming protons fuse, one can calculate an upper limit for the fusion reaction rate from Eq. (3) using the reactivities at the given energies: 1.7×10^{-23} m^3/s at 1 MeV and 3.9×10^{-24} m^3/s at 0.4 MeV. This yields a reaction rate of 5.1×10^{32} m^{-3}s^{-1} for the fast and 0.9×10^{32} m^{-3}s^{-1} for the slow protons. Hence, the theoretical upper limit for fusion processes in this kind of reactor is 6×10^{32} m^{-3} s^{-1} per laser shot. If the lithium target is thick enough and all of the incoming fuse, the obtainable energy is $1.15 \times 10^{15} \times 17.2$ MeV $\times 1.6 \times 10^{-19} \approx 3.16$ kJ. However, it has to be noted that this value alone is too low to reach the energetic break-even with this setup, since the experiments from which the data was taken lists an laser-ion conversion efficiency of about 5%. On the other hand, these experiments were not tailored for proton-lithium fusion and there should be much room for improvement. Furthermore, typical sub nanosecond laser systems have repetition rates of up to 10 Hz, which gives energy yields of 31.6 kJ per second. Other experimentalists, such as Brenner et al. [18] measured a proton acceleration efficiency of 15% for similar fusion relevant conditions (solid target, proton energies 5–30 MeV). Reaching this value in laser-proton acceleration efficiency would already increase the energy output up to around 100 kJ per second. Taking all these numbers into account yields an estimation of an energy gain $Q \approx 167$ in the ideal case. To further enhance the efficiency of such a fusion reactor, it is suggested to use hybrid targets that are made of boron and lithium. This enables to make the optimal use of proton beams with a certain energy spread as can be seen in the following Fig. 5:

It is evident that especially in the energy range between 2 and 3 MeV there is almost a doubling of the achievable fusion output. Unfortunately, data for proton-boron fusion cross sections couldn't been found for energies greater than 3.3 MeV.

Another important entity for designing an optimised fusion target is the penetration depth $R(E)$ of the proton beam into the target. This can be calculated via the semi-empirical equation given by Burrell [19]:

$$R(E) = \frac{1.53 \times 10^{-3} + 2.33 \times 10^{-4}\sqrt{A}}{1.6 \times 10^{-6} + 10^{-6}\sqrt{Z}} \times$$
$$\times \ln\left[1 + (1.6 \times 10^{-6}\sqrt{Z})E^{1.78}\right] \quad (6)$$

Here Z denotes the atomic number, A is the mass number and E is the energy of the incoming proton beam. This equation has an accuracy of $\pm 5\%$ for $Z < 20$. The results of the calculation is shown in the next Fig. 6:

The penetration depth for a monoenergetic proton beam lies between 330 microns for lithium and 400 microns for boron. If the penetration occurs at the energies related to the peaks in the fusion cross
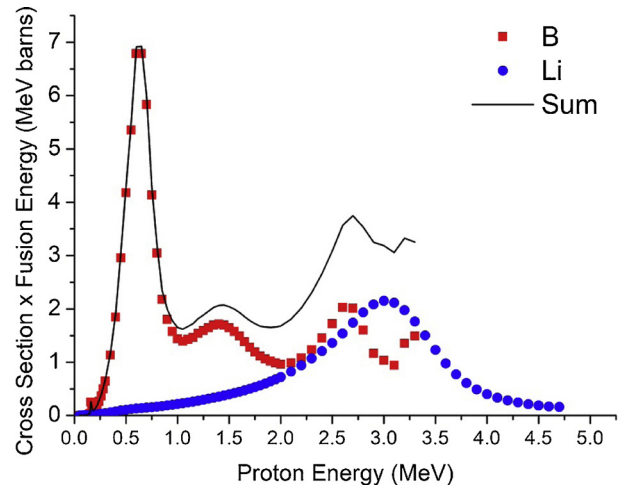

Fig. 5. Products of fusion yield and cross section area for lithium (blue) and boron (red) targets and the sum between the two (black).
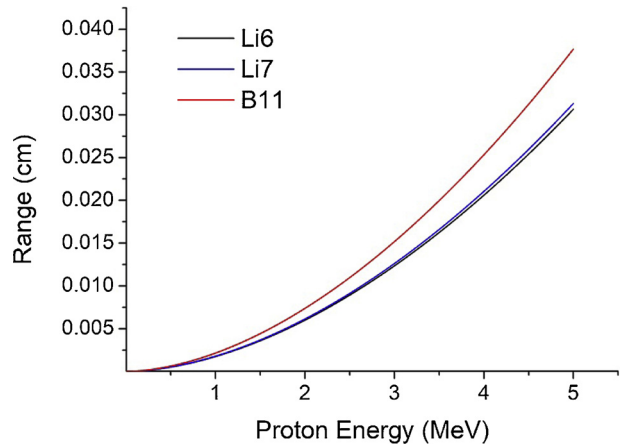

Fig. 6. Proton penetration depth as a function of the beam energy in B (red), ^{6}Li (black) and ^{7}Li (blue).

section, the values for the proton range are 4 micron at 0.4 MeV and 110 micron at 2.5 MeV for boron and about 120 micron at 3 MeV for Li.

It has to be emphasised at this point that the distance between the proton source and the LiB target is, in principle, arbitrary as long as the proton beam can be collimated. For example, in Ref. [1] a distance of 1 m was assumed and the necessary properties for collimation magnets were discussed. Such a long distance has the big advantage of avoiding steep temperature gradients between the hot LiB target and a liquid hydrogen proton source.

4. Geometry of a cryogenic hydrogen based proton source

Since the cryogenic hydrogen source acts as a target for the laser beam, it is useful to also discuss possible geometries for it. In this work a solid hydrogen [20] proton source with an elliptical cross section is compared to one with a cuboid shape. The former is similar to the cylindrical one that was used in a recent experiment [21]. It will act like a convex lens and can correct the natural divergence of the incoming laser beam and generate a more homogeneous proton energy distribution [21]. The latter is preferable in the case of an incoming laser beam with small numerical aperture (NA). A sketch of a setup with a hydrogen lens is shown in the following Fig. 7:

It is evident that the incoming photons may be either absorbed or backscattered. In both cases the photons will transfer some of their momentum onto the electrons upon ionization and will accelerate them
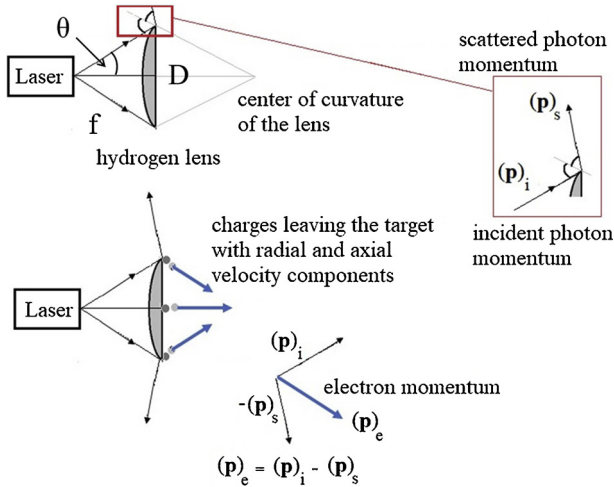
Fig. 7. Sketch for a lens shaped cryogenic hydrogen proton source. $p_{e,i,s}$ are the momentum vectors of the electrons, incident and scattered photons, respectively.

outwards. The direction of the electron momentum is defined by the difference in the momentum vector of the incident and scattered photons, respectively. The protons are then, in turn, accelerated by the electric field created by the leaving electrons. Since the inverse of the focal length of a lens as depicted in Fig. 7 is given by:

$$f^{-1} = (n-1) \cdot \left(\frac{1}{R_1} - \frac{1}{R_2} + \frac{(n-1)d}{nR_1R_2} \right) \qquad (7)$$

where R_1 and R_2 denote the radius of curvature of the left and right hand side of the lens. Thus, the diameter to radius ratio of a solid hydrogen lens can be calculated with the numerical aperture of the incoming laser beam, which is defined by:

$$N_A = \sin[\tan^{-1}(\frac{D}{2f})] \approx \frac{D}{2f} \qquad (8)$$

For the setup in Fig. 7 $R_1 = R$ and $R_2 = \infty$. Thus $f = \frac{R}{n-1}$ and

$$\frac{D}{R} = \frac{2N_A}{n-1} \qquad (9)$$

It is evident from Eq. (9) that the curvature and diameter of a cryogenic hydrogen lens will have an influence on the trajectories of the photons and charged particles. As the refractive index of cryogenic hydrogen is 1.13 and nearly independent of the wavelength in the region of 400–1100 nm [22] and a typical numerical aperture for the laser beam is 0.29, the diameter to radius ratio of the solid hydrogen target is 4.46 in our example.

On the other hand, for an incoming laser beam that has a smaller numerical aperture or is perfectly parallel, the physical situation changes drastically as shown in the following Fig. 8.

It can be seen that a lens shaped proton source will create an inhomogeneous charge density profile when hit by a parallel laser beam. This is due to the greater thickness in the center of the 'lens', where more hydrogen atoms are available for ionisation than on the edges. The resulting charge density gradient will induce radial currents, which might lead to a variety of instabilities in the proton beam. One example is the magneto rotational instability (MRI) that occurs due to the Lorentz force acting on the charge carriers in the radial electrical currents. The MRI can lead to beam distortions when the protons enter an external magnetic field as it is typically used for focusing the beam in laser-proton acceleration experiments. Furthermore, a cuboid hydrogen target leads to a smaller spreading of the outgoing proton beams as depicted on the r.h.s of Fig. 8. The reason for the increased spreading for the lens-shaped target is the enhanced electric field sensed by protons with a radial velocity component as shown in Fig. 7. In the case of

a lens-shaped target, almost all protons that exit the back of the lens have such a radial component of velocity. These protons experience a Lorentz force $\vec{F}_L = q(\vec{E} + \vec{v} \times \vec{B})$ in the magnetic field, which causes an additional tangential electric field $\vec{E}_t = \vec{v} \times \vec{B}$, which together with the electrostatic field $\vec{E}_r$ caused by the proton distribution within the beam, leads to a larger $\vec{E}_{\text{tot}}$ for the protons with a radial component of the velocity. Ultimately, the proton beam spreads out more due to this enhanced $\vec{E}_{\text{tot}}$.

In order to further investigate the behaviour of the proton beam PIC code simulations have been performed with 100 protons, which start off the back of the proton source based on the incoming photon beam profile. The number of protons was taken to be constant throughout the simulation (no subsequent electron capture assumed) and the screening effect of electrons is neglected. Using 1 proton per cell, it was assumed that along the horizontal direction, the motion is linear with constant speed and the kinetic energy is 1 MeV for each proton. In the perpendicular direction Coulomb interactions between the closest 8 neighbors of each proton was taken into account. Then the increase in the perpendicular speed from the electrostatic energy exchange with the closest 8 neighbors of each proton was calculated. The proton source and the initial proton beam diameter was taken to be ≈ 5 mm for the PIC code simulations based on data described in [23]. The results of the numerical calculations are shown in Figs. 8 and 9:

The blue line is the envelope of the curves that run perpendicular to the total velocity of a proton (averaged over 8 cells). Each line illustrates a different moment of the temporal evolution of the proton beam. Given the large speed on the horizontal direction, the spreading of the proton beam is not large at this short distance from the target because the speed in the perpendicular direction amounts to just 0.1 MeV. But for more protons in the beam, the electrostatic interaction increases.

5. Design of a lithium-boron hybrid target

In order to maximise the fusion output we propose a lithium-boron hybrid target that compensates the energy spread of the incoming proton beam to some extend by taking advantage of the very different peaks in the fusion cross sections of these materials. The easiest way to achieve this is a system of lithium and boron foils that are embedded in a actively cooled steel case. This case has an orifice on top through which the proton beam can enter and can be opened in order to simply replace the Li–B fuel after it is burned up. The proton beam enters the casket from the top, which allows to handle molten Li without problems. The melting of the lithium is expected since the envisioned fusion reactions will produce a significant amount of heat. A schematics of such a hybrid target is presented in Fig. 10:

As to be seen from Fig. 5 boron has its maximum fusion yield at much lower proton energy than lithium. This means that protons with an initial kinetic energy of, for example, three to four MeV can penetrate a thin lithium foil, lose some of their energy and are still able to fuse efficiently with boron. Hence, it is suggested that the top layer of the hybrid LiB target should be made of a lithium foil of around 200 micron thickness. A comparison with Fig. 6 shows that after traversing this distance in lithium the protons will have lost about 1–1.5 MeV. Thus, they will just have enough energy to undergo fusion with atoms in the boron layer underneath. The thickness of the boron layer should be in the same order of magnitude. The number of individual layers is arbitrary. However, more layers will enhance the operation time of the LiB target, since the lithium and boron will be over time consumed due to the fusion reactions. Recent results show that magnetic focusing of up to 10^{18} cm^{-3} charged particles down to 5 microns is possible [24]. Thus, an entrance orifice diameter of about 1 mm is sufficient for the protons to enter the target. This ensures a highly improved efficiency in terms of aneutronic fusion rates. Furthermore, such a multi layered system will increase the lifetime of the target considerably and it is easy to be replaced. The heat from the fusion reactions is supposed to melt
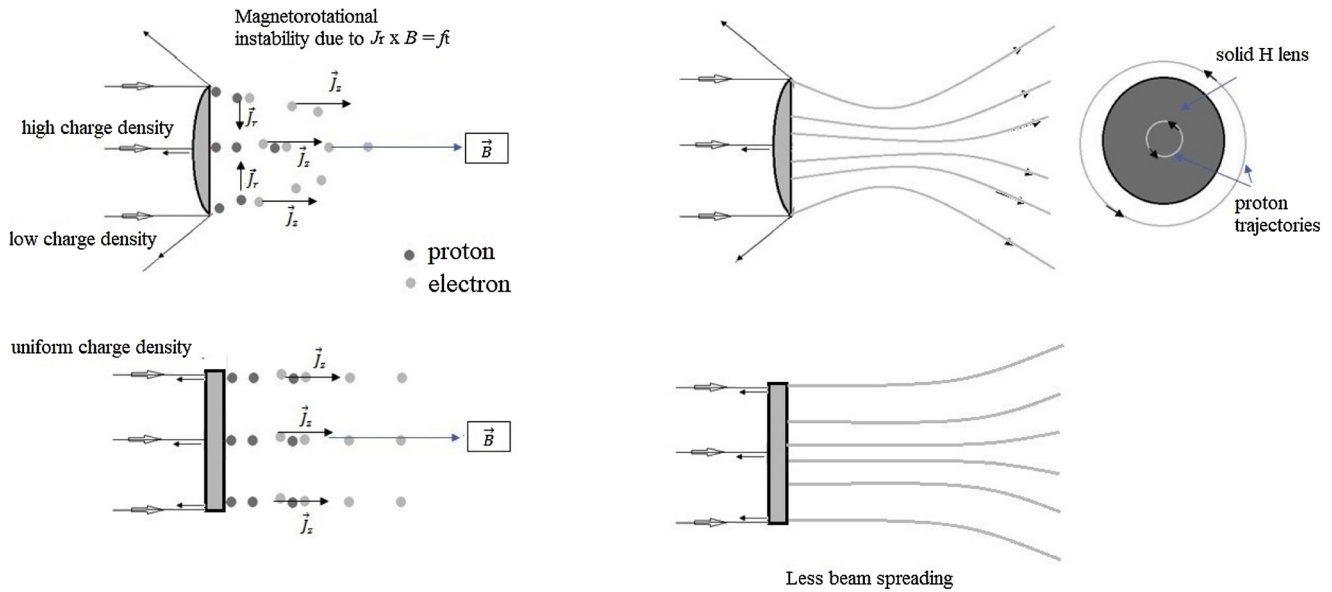
Fig. 8. Comparison between two possible hydrogen target shapes in the presence of a beam focusing external magnetic field (left) and their corresponding beam spreading behaviour (right).
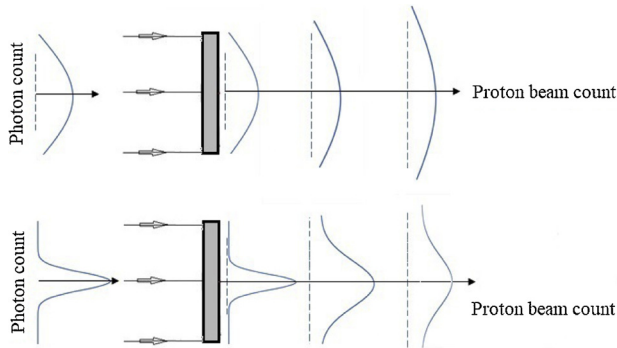

Fig. 9. Comparative PIC code simulations of the axial proton beam density profiles for two different laser intensity profiles.
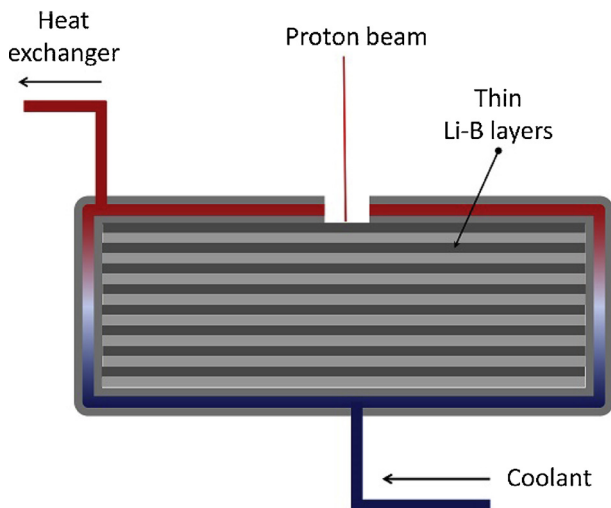

Fig. 10. Multilayered lithium-boron (LiB) fusion target with active cooling.

the lithium while the boron stays solid due to its much higher melting point. This thermal energy will be used to heat up the coolant inside the target casket wall, which will create steam to drive a turbine.

6. Conclusions

In this paper we compared several experimental data from laser-proton acceleration experiments as well as different types of targets and proton sources that are relevant for aneutronic fusion. The most promising proton source in terms of high proton yield at comparatively low laser power is cryogenic hydrogen. For this type of source different geometries were compared and discussed. It was argued that a lens shaped cryogenic hydrogen ribbon offers a more homogeneous proton energy distribution in the beam and can correct the natural divergence of the laser beam. A flat ribbon, on the other hand, minimizes the beam spreading and is easier to be produced as a rectangular orifice for the hydrogen extruder is less complicated than a perfectly elliptic one. Additionally, some important physical properties of the fusion targets were examined. It was argued that the most promising target is a hybrid of boron and lithium as it enables to get a maximum fusion yield even if the energy spread of the accelerated protons is large. In fact, with such a hybrid target the permissible proton energy can be somewhere between 0.4 and 4 MeV in order to achieve a notable number of fusion reactions. It was also shown via calculations of the proton penetration depth that most of the fusion reactions will occur in the first few 100 μm below the boron-lithium target surface. When the top layer of the LiB hybrid target is made of lithium while the following one consists of boron and so on, a maximum number of fusion reactions can be achieved in such a type of aneutronic reactor. The heat from the fusion reactions will be used to actively cool the LiB target container and to produce steam for a suitable turbine.

References

[1] J. Gruenwald, Proposal for a novel type of small scale aneutronic fusion reactor, Plasma Phys. Control. Fusion 59 (2) (2017) 025011 http://stacks.iop.org/0741-3335/59/i=2/a=025011.

[2] P.T. Farnsworth, Method and Apparatus for Producing Nuclear-Fusion Reactions, (1968) http://www.google.com/patents/US3386883.

[3] R.L. Hirsch, Inertial-electrostatic confinement of ionized fusion gases, J. Appl. Phys. 38 (11) (1967) 4522–4534.

[4] R. Bowden-Reid, J. Khachan, J.-P. Wulfkühler, M. Tajmar, Evidence for surface fusion in inertial electrostatic confinement devices, Phys. Plasmas 25 (11) (2018) 112702, https://doi.org/10.1063/1.5053616.

[5] H.W. Davison, Compilation of Thermophysical Properties of Liquid Lithium, (1968).

[6] V. Zerkin, EXFOR Database, (2018) https://www.nds.iaea.org/exfor/.

[7] S.N. Abramovich, B.J. Guzhovskij, V.A. Zherebcov, A.G. Zvenigorodskij, Estimated values of total and differential cross sections of proton interactions with nuclei Li-6

and Li-7, Vop At Nauki i Tekhn Ser Yad Konstanty 114 (1984) 17.

[8] R.C. Weast (Ed.), Handbook of Chemistry and Physics, 56th ed., CRC Press, 1975.

[9] M. Chiari, L. Giuntini, P.A. Mandò, N. Taccetti, Proton elastic scattering cross-section on boron from 0.5 to 3.3 MeV, Nucl. Instrum. Methods Phys. Res. Sect. B: Beam Interact. Mater. Atoms 184 (3) (2001) 309–318.

[10] A.J. Charlotte, N.P. Palmer, I. Dover, M. Pogorelsky, G.I. Babzien, M. Dudnikova, M.N. Ispiriyan, J. Polyanskiy, P. Schreiber, V. Shkolnikov, Z. Yakimenko, Najmudin, Monoenergetic proton beams accelerated by a radiation pressure driven shock, Phys. Rev. Lett. 106 (2011 Jan) 014801, https://doi.org/10.1103/PhysRevLett.106.014801.

[11] A. Sharma, Z. Tibai, J. Hebling, Intense tera-hertz laser driven proton acceleration in plasmas, Phys. Plasmas 23 (6) (2016) 063111.

[12] M.H. Helle, D.F. Gordon, D. Kaganovich, Y. Chen, J.P. Palastro, A. Ting, Laser-accelerated ions from a shock-compressed gas foil, Phys. Rev. Lett. 117 (2016 Oct) 165001, https://doi.org/10.1103/PhysRevLett.117.165001.

[13] J.T. Morrison, S. Feister, K.D. Frische, D.R. Austin, G.K. Ngirmang, N.R. Murphy, C. Orban, E.A. Chowdhury, W.M. Roquemore, Mev proton acceleration at kHz repetition rate from ultra-intense laser liquid interaction, New J. Phys. 20 (2) (2018) 022001.

[14] M. Gauthier, J.B. Kim, C.B. Curry, B. Aurand, E.J. Gamboa, S. G“ode, C. Goyon, A. Hazi, S. Kerr, A. Pak, et al., High-intensity laser-accelerated ion beam produced from cryogenic micro-jet target, Rev. Sci. Instrum. 87 (11) (2016) 11D827.

[15] A. Maksimchuk, S. Gu, K. Flippo, D. Umstadter, V.Yu. Bychenkov, Forward ion acceleration in thin films driven by a high-intensity laser, Phys. Rev. Lett. 84 (2000 May) 4108–4111, https://doi.org/10.1103/PhysRevLett.84.4108.

[16] D. Khaghani, M. Lobet, B. Borm, L. Burr, F. G”artner, L. Gremillet, L. Movsesyan, O. Rosmej, M.E. Toimil-Molares, F. Wagner, et al., Enhancing laser-driven proton acceleration by using micro-pillar arrays at high drive energy, Sci. Rep. 7 (1) (2017) 11366.

[17] D. Margarone, A. Velyhan, J. Dostal, J. Ullschmied, J.P. Perin, D. Chatain, S. Garcia, P. Bonnay, T. Pisarczyk, R. Dudzak, M. Rosinski, J. Krasa, L. Giuffrida, J. Prokupek, V. Scuderi, J. Psikal, M. Kucharik, M. De Marco, J. Cikhardt, E. Krousky, Z. Kalinowska, T. Chodukowski, G.A.P. Cirrone, G. Korn, Proton acceleration driven by a nanosecond laser from a cryogenic thin solid-hydrogen ribbon, Phys. Rev. X 6 (2016 Nov) 041030, https://doi.org/10.1103/PhysRevX.6.041030.

[18] C.M. Brenner, A.P.L. Robinson, K. Markey, R.H.H. Scott, R.J. Gray, M. Rosinski, O. Deppert, J. Badziak, D. Batani, J.R. Davies, et al., High energy conversion efficiency in laser-proton acceleration by controlling laser-energy deposition onto thin foil targets, Appl. Phys. Lett. 104 (8) (2014) 081123.

[19] Martin O. Burrell, The Calculation of Proton Penetration and Dose Rates, (1964).

[20] S. Garcia, D. Chatain, J.P. Perin, Continuous production of a thin ribbon of solid hydrogen, Laser Part. Beams 32 (4) (2014) 569–575.

[21] L. Obst, S. Göde, M. Rehwald, F.-E. Brack, J. Branco, S. Bock, M. Bussmann, T.E. Cowan, C.B. Curry, F. Fiuza, et al., Efficient laser-driven proton acceleration from cylindrical and planar cryogenic hydrogen jets, Sci. Rep. 7 (1) (2017) 10248.

[22] M. Perera, Brian A. Tom, Y. Miyamoto, M.W. Porambo, L.E. Moore, W.R. Evans, T. Momose, B.J. McCall, Refractive index measurements of solid parahydrogen, Opt. Lett. 36 (6) (2011) 840–842, https://doi.org/10.1364/OL.36.000840.

[23] S. Busold, D. Schumacher, O. Deppert, C. Brabetz, S. Frydrych, F. Kroll, M. Joost, H. Al-Omari, A. Blažević, B. Zielbauer, et al., Focusing and transport of high-intensity multi-mev proton bunches from a compact laser-driven source, Phys. Rev. Spec. Top. Accel. Beams 16 (10) (2013) 101302.

[24] S. Steinke, J. Van Tilborg, C. Benedetti, C.G.R. Geddes, C.B. Schroeder, J. Daniels, K.K. Swanson, A.J. Gonsalves, K. Nakamura, N.H. Matlis, et al., Multistage coupling of independent laser-plasma accelerators, Nature 530 (7589) (2016) 190–193.